

EXPLORING MATHEMATICAL ASPECTS OF ALGORITHMS FOR CHALLENGING TOPICS IN NUMERICAL ANALYSIS

Vladimir V. Riabov

Rivier University

420 S. Main Street • Nashua, NH 03060-5086 • USA • E-mail: vriabov@rivier.edu

Mathematical models and numerical algorithms are explored for several technological challenges in physics, chemistry, aerothermodynamics, and evolution of dynamic systems in economics and weather forecast. Various mathematical concepts are examined to evaluate multifold integrals, dynamics of strange attractors, and solutions of differential equations with small parameters at the highest derivatives.

1. Introduction

A course on Numerical Methods typically covers introductory topics in numerical analysis for students of engineering, science, mathematics, and computer science who have completed elementary calculus, linear algebra and matrix theory. The course is usually limited to exploring basic algorithms [1] for solving traditional simple problems in sciences and engineering. As a result, the students have become inadequately prepared to construct proper mathematical models and explore more sophisticated algorithms of modern technological challenges. To reduce this gap, the author has offered a series of case studies [2], which provide concrete examples of the ways numerical methods lead to solutions of some scientific problems. The similar approach was promoted in [3].

Topics involve familiarity with Math concepts that are not often taught, or inadequately covered, including differential equations with singularities, Monte-Carlo simulation, asymptotic theory, attractors, and theories of chaos, instabilities, and catastrophes. Students demonstrate usually a lack of experience and knowledge of how to develop an adequate math model for a complex scientific or engineering problem. Therefore, we encourage all students to strengthen their abilities in various problem-solving techniques.

The numerical analysis course material is likely to change rapidly. Just staying up to date with the latest threats and techniques is a real challenge for both an instructor and a student, and can consume large amounts of time and resources [2, 3].

2. Estimations of Multifold Integrals

Many technological problems (e.g., calculations of transport coefficients and chemical-reaction rates) require estimations of multifold integrals under the conditions when classical Newton-Cotes formulas for numerical integration [1, 3] could not be applied. Instead, Monte-Carlo simulation methods [4, 5] could be effectively used. In the first case study, students analyzed the rotational relaxation of a gas of homonuclear diatomic molecules. The realistic model of the intermolecular interaction [6] was used for calculating the redistribution of the rotational and translational energies upon collision.

The process of establishing equilibrium with respect to the rotational degrees of freedom in terms of the τ -approximation can be described by the relaxation equation Eq. (1) [7] with the following parameters (see Eq. 2 [7]) that determine the relaxation time τ_{R1} :

$$\frac{d \varepsilon_R}{d t} = \frac{(\varepsilon_R^0 - \varepsilon_R)}{\tau_{R1}} \quad (1)$$

$$\frac{1}{p \tau_{R1}(T)} = \frac{2}{\pi^2 \sqrt{2 \pi \mu k T}} \int_0^{r_0} \int_0^\infty \int_0^\pi \int_0^\pi \int_{-\infty}^{+\infty} \int_{-\infty}^{+\infty} \Delta E^2 \quad (2)$$

$$\times \exp \left(-\frac{g^2 + p_i^2 + p_j^2}{2} \right) b db \frac{g^7}{16} dg d\varphi_i d\varphi_j dp_i dp_j$$

The expression for the energy $\Delta E = \Delta E_N / \mu v^2 / 2 = \Delta E_i + \Delta E_j$ transferred at the time of collision from the translational to the rotational degrees of freedom takes the form:

$$\Delta E_i = \frac{128 \pi^2 \varepsilon^2 l_i^2 \sin^2 2\psi_i}{\alpha^4 d^2 g^2 sh^2 \kappa_i} - \frac{16 \sqrt{2} \pi \varepsilon p_i l_i \sin 2\psi_i}{\alpha^2 d g^2 sh \kappa_i} \quad (3)$$

Here the following analytic expressions for the resulting angular velocities of the molecules are used [7]:

$$\varphi_i = -\frac{16 \pi l_i \sin 2\psi_i}{\alpha^2 d^2 sh^2 \kappa_i} \quad (4)$$

$$\kappa_i = \frac{2 \pi l_i}{\alpha g \sqrt{1 - q^2 + \frac{2 \varepsilon_0}{g^2 k T}}} \quad (5)$$

$$\psi_i = \varphi_i - \arcsin q; \quad q = \frac{b}{r_0} \quad (6)$$

$$l_i = \sqrt{2} p_i d - \frac{q g}{r_0}; \quad g = \sqrt{\frac{\mu}{k T}} v \quad (7)$$

where p_i and φ_i are the initial reduced angular momenta and initial phases counted from the direction of the initial velocity of relative motion of the molecules, and various molecular interactive parameters have been defined in Refs. 6 and 7.

To estimate the rotational relaxation time, the sixfold integrals were calculated at 200 points over the range of temperatures from 200 K to 10,000 K, using the Monte Carlo

simulation technique [5], with 4000 tests at each point. The data for intermediate points were determined by means of the interpolation technique using cubic splines of defect 1 with smoothing. The accuracy of the calculations was estimated as 1.5%. The experimental data (filled squares) [8, 9] for molecular nitrogen correlates well with the numerical results (empty squares) as shown in Fig. 1.

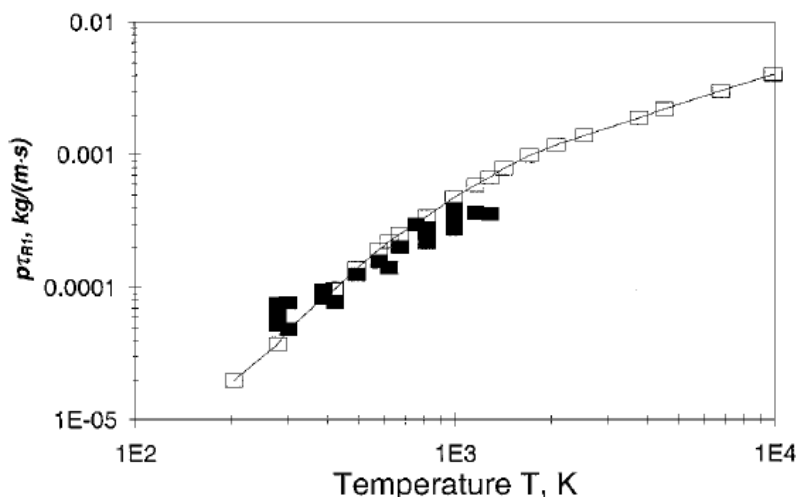


Figure 1. Parameter $p\tau_{R1}(T)$ as a function of temperature: \square , solution of Eq. (2) at the molecule parameter $d^* = 0.62$ [6]; and \blacksquare , experimental data [8, 9].

3. Solving Singular Differential Equations

Various problems of applied mathematics, thermophysics, and aerodynamics (e.g., stability of mechanical systems and flow boundary layers, fuel combustion, and heat protection of spacecraft) come to solving differential equations with small coefficients at the highest derivatives. This phenomenon leads to the formation of regions with small linear dimensions where gradients of functions are large. The numerical analysis of such problems by traditional box-schemes is restricted by non-uniform convergence or even divergence of numerical solutions. In this case study, the numerical solutions of the model singular ordinary differential equation have been evaluated for the linear boundary value problem [10]. The developed numerical method [11, 12] was used for the analysis of gas flow parameters in boundary and viscous shock layers under the conditions of blowing on the body surface and nonequilibrium chemical reactions.

From a mathematical point of view, the increase of the flow rate of blowing gas or chemical-reaction rates is equivalent to the existence of a small coefficient at the highest derivative in the boundary-layer equations [10]. A sublayer (of uncertain location) with large gradients of functions is created. The gas flow in the boundary layer was studied using a two-point exponential box-scheme and an effective regularization algorithm [11]. The uniform second-order convergence was obtained for functions and derivatives in the full range of small parameters such as blowing factors and inverse chemical-reaction rates. The approach could be applied to boundary layers with gas injection and combustion [10, 11].

3.1. The Model Linear Boundary Value Problem

In general, the method is designed for solving the following model equation:

$$\varepsilon u'' + au' - bu = d \quad (8)$$

Here the parameter ε can accept very small magnitudes, and $a \geq 0, b \geq 0$. The solution of the equation (8) with constant coefficients is the following [11, 12]:

$$u = Ae^{\alpha\eta} + Be^{\gamma\eta} + \psi, \quad \psi = \frac{d}{\varepsilon\alpha\gamma} \quad (9)$$

$$\alpha = -\frac{a}{2\varepsilon} + \sqrt{\frac{a^2}{4\varepsilon^2} + \frac{b}{\varepsilon}} \quad (10)$$

$$\gamma = -\frac{a}{2\varepsilon} - \sqrt{\frac{a^2}{4\varepsilon^2} + \frac{b}{\varepsilon}} \quad (11)$$

where A and B are arbitrary constants, and η is the main variable parameter.

The solution (9-11) is used to obtain the box-scheme characteristics by considering that the functions as well as the derivatives are continuous in the cells [10, 11]. The two-point uniform exponential box-scheme was introduced in [11]. The identical problem was considered in [12] by using a three-point exponential box-scheme.

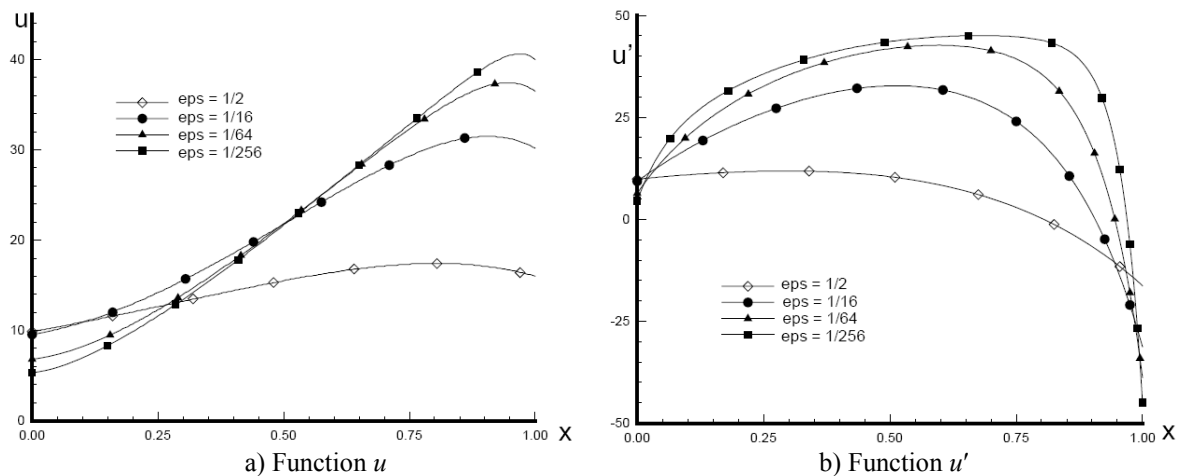


Figure 2. Functions u and u' as solutions of the linear boundary-value problem (12-14).

The linear boundary value problem is studied for the following model singular ordinary differential equation [13] and boundary conditions:

$$\varepsilon u'' - (1 + x^2)u = -(4x^2 - 14x + 4)(1 + x)^2 \quad (12)$$

$$u(0) - u'(0) = 0 \quad (13)$$

$$u(1) + u'(1) = 0 \quad (14)$$

The numerical solutions of the equation (12) with boundary conditions (13) and (14) have been calculated by using the two-point exponential box-scheme [11]. The results for the function u and its derivative u' are shown in Fig. 2. At various parameters ε , they demonstrate the formation of thin regions where gradients of functions are large.

3.2. Gas Blowing into a Boundary Layer

Consider the perfect-gas flow in the boundary layer (BL) near the stagnation point of a blunt body with uniform blowing at the surface [14]. The system of BL equations acquires the following form [10, 15]:

$$U'' + fU' + \beta(S + 1 - U^2) = 0 \quad (15)$$

$$f' = U' \quad (16)$$

$$S'' + \sigma fS' = 0 \quad (17)$$

where the Faulkner-Scan constant [14] $\beta = (1 + j)^{-1}$ characterizes the pressure gradient in inviscid flow; $j = 0$ or 1 in plane and axisymmetric cases correspondingly; and $\sigma = 0.72$ is the Prandtl number.

Boundary conditions are the following:

On the body surface ($Y = 0$) considering the gas blowing:

$$f = f_w = \text{const}, \quad U' = 0, \quad S = S_w \quad (18)$$

On the external boundary of the layer ($Y \rightarrow \infty$):

$$U = 1, \quad S = 0 \quad (19)$$

In Eq. (18) the parameter f_w characterizes the mass flow rate of the blowing gas. Special box-schemes with uniform convergence [16] or exponential schemes [10, 12] should be used in order to solve the problem at large $|f_w|$. The principal advantages of the two-point box-schemes are: 1) any type of boundary conditions "estimated" accurately [11]; 2) algorithmic changes of the grid-cell are simple [17]; and 3) fluxes of the flow parameters are calculated without additional procedure [11], and the approximation error of the fluxes is the same as that of other terms of the equations. The two-point exponential box-scheme developed [10] has the second order of uniform convergence. The scheme and its regularization algorithm [11] have been used for the numerical

solution of Eqs. (15)-(19) under the conditions of moderate and intensive blowing from the thermally isolated body surface ($S_w = 0$). The profiles of the tangential component of the velocity U and its derivative U' along the normal at the stagnation point on the surface of the axisymmetrical blunt body ($\beta = 0.5$) are shown in Fig. 3 for various blowing parameters ($f_w = 0, -2.5, -10, -25$). The presence of the blowing flow significantly changes the flow structure. As the rate of blowing increases, the boundary layer becomes thicker, and the friction on the body surface decreases.

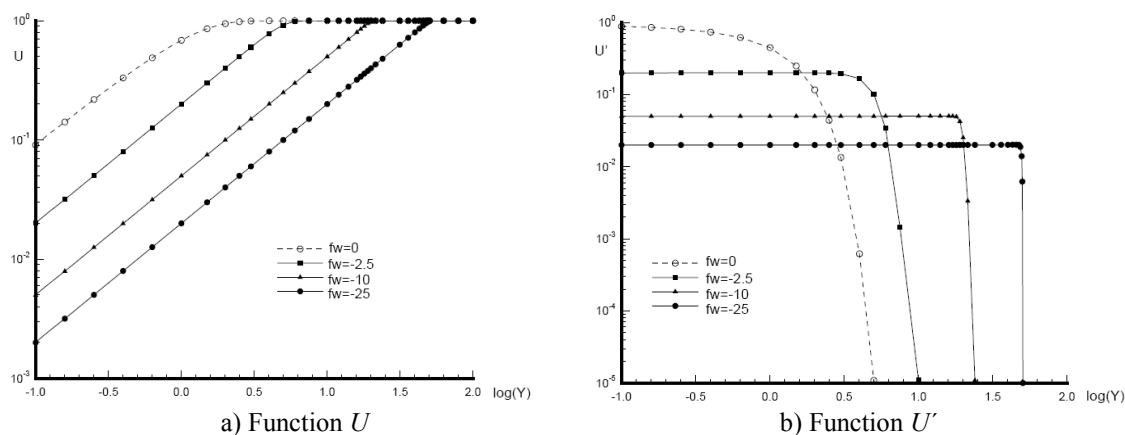


Figure 3. Functions U and U' across the boundary layer for various blowing factors.

4. Exploring Algorithms for Uniform Calculations of Flows under Various States

The purpose of the fourth case study was to analyze heat-transfer processes at the catalytic materials of the shock-tube end after shock wave refraction in terms of the model of the nonsteady-state nonequilibrium thermal boundary layer [18]. The major challenge was to develop the algorithm that could correctly and uniformly calculate flow parameters under all possible states (chemically “frozen”, nonequilibrium, and equilibrium ones) right behind the moving reflected shock wave. The types of governing differential equations are significantly different in these three cases, and the algorithm should automatically “adapt” to these changes across the flow.

4.1. Gas Flow behind the Incident Shock Wave

Students considered the simplest model [18, 19] of the one-dimensional inviscid dissociating gas flow behind the incident shock wave, which propagated in an ideal air with parameters of pressure $p_1 = 1$ and 100 Pa, and temperature $T_1 = 295$ K at constant velocity $U_S = 5$ km/s. The system of chemical reactions occurring in the five-component mixture and reaction constants used in the present study was described in [20].

The algorithm of calculation of the parameters behind the incident and reflected shock waves was described in [18] in detail. The system of algebraic-differential equations [19] was solved at each point of the flow field behind the incident shock wave under the assumption that air is not dissociated on the shock wave front. A modified Newton's

method [21] with optimal choice of iteration step was used for numerical solution of the equations. The flow parameters behind the incident shock wave are shown in Fig. 4 (*left*). The solutions obtained for temperature and pressure are typical for dissociating gas flows with nonequilibrium relaxation [19, 22, 23]. For small time interval ($t \approx 10^{-8}$ sec) the gas state is frozen [19], while at large distances from the shock wave (at $t \geq 10^{-5}$ sec and $p_1 = 100$ Pa) the flow parameters tend to their limiting equilibrium values [18]. With decrease in initial pressure up to $p_1 = 1$ Pa the equilibrium state is reached at significantly distances, while at $t < 10^{-5}$ sec the flow parameters differ little from frozen.

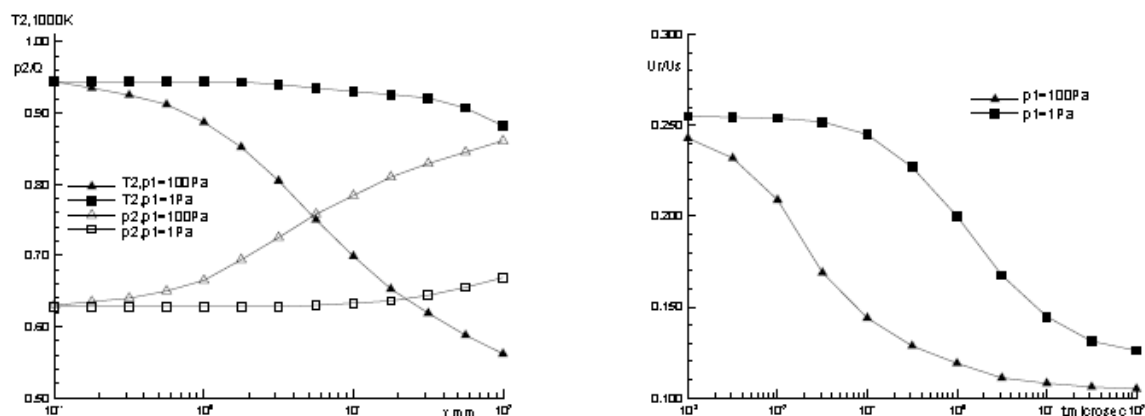


Figure 4. Temperature T_2 and pressure p_2 behind the incident shock at distances from the wave front (*left*), and velocity of the reflected shock wave U_R as a function of time (*right*) at various initial pressure parameters: $p_1 = 1$ Pa (squares) and $p_1 = 100$ Pa (triangles).

4.2. Gas Flow behind the Reflected Shock Wave

The reflected shock is propagated in the disturbed field after the incident shock [23]. The velocity of the reflected shock wave U_R as a function of time, for two cases of pressure $p_1 = 1$ and 100 Pa, is plotted in Fig. 4 (*right*) (squares and triangles, correspondingly). The decrease of values U_R indicates the nonequilibrium type of chemical reactions behind the incident shock wave [23]. The magnitude of pressure p_1 defines the time required for attainment of the steady-state distribution. This time is less by approximately a factor of 100 for $p_1 = 100$ Pa. Therefore, the parameter U_R can be used for experimental verification of nonequilibrium states in the areas behind the shock and near the tube end.

Using the computational technique [19], the distribution of temperature T_3 and pressure p_3 behind the reflected shock wave was calculated. The computational results are shown in Fig. 5 (*left*) at the same cases of the initial pressure p_1 . The distribution of temperature T_3 [see Fig. 5 (*left*)] is similar to the distribution of U_R and it can be used for the identification of the type of chemical processes behind the shocks [18, 23]. Figure 5 (*left*) presents also the computational results for pressure $p_3(t)$ behind the reflected shock. This parameter is the most conservative one. Nevertheless, for the large value of initial pressure $p_1 = 100$ Pa (triangles) the significant increase of the values p_3 is observed after the short initial time-interval of decreasing. This is a result of the influence of different types of chemical processes behind the incident wave with initial pressure p_1 [19, 23].

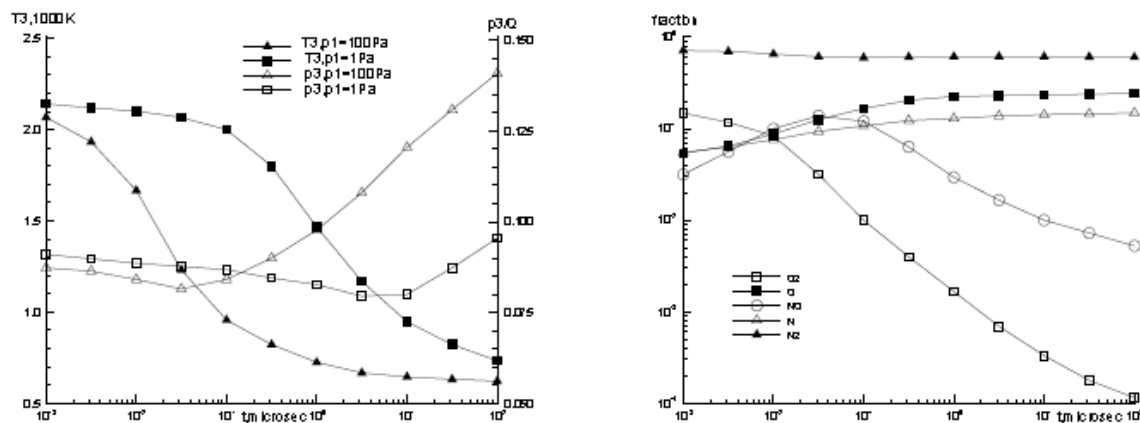


Figure 5. Temperature $T_3(t)$ and pressure $p_3(t)$ behind the reflected shock wave at various initial pressure parameters: $p_1 = 1$ Pa (squares) and $p_1 = 100$ Pa (triangles) (left), and mass fractions α_i in air behind the reflected shock wave at $p_1 = 100$ Pa (right).

At $p_1 = 100$ Pa, the flow behind the reflected shock is close to a state of local thermodynamic equilibrium [18], while at $p_1 = 1$ Pa, the flow is significantly nonequilibrium [19, 23]. The function $p_3(t)$ can be used for the prediction of pressure in the thermal viscous layer near the tube end, and it correlates with the value of pressure $p_w(t)$ at the tube end. Additional important information is the distribution of air components α_i behind the reflected shock wave shown in Fig. 5 (right).

5. Numerical Modeling of Strange Attractors

The course topics cover mathematical foundations of evolution of dynamic systems that could be described in terms of strange attractors. The case studies examine numerical modeling of chaotic dynamic systems [24] (turbulence, weather forecast, and economic system development). They were introduced through classical examples of bifurcations of systems modeling equilibrium in chemical reactions, socio-economy (*Rössler attractor*) and atmospheric dynamics (*Lorenz attractor*) [25].

The Lorenz attractor was first studied by E. N. Lorenz in [25]. It was derived from a simplified model of convection in the Earth's atmosphere. The system is most commonly expressed as the following three coupled non-linear differential equations:

$$dx / dt = a (y - x) \quad (20)$$

$$dy / dt = x (b - z) - y \quad (21)$$

$$dz / dt = xy - c z \quad (22)$$

Here (x, y, z) are the Cartesian coordinates, " t " is the time variable, " a " is the Prandtl number, " b " is the Rayleigh number, and " c " is the system parameter. The series does not form limit cycles nor does it ever reach a steady state (see Fig. 6). Instead, it is an example of deterministic chaos. As with other chaotic systems, the Lorenz system is sensitive to the initial conditions: two initial states no matter how close will diverge.

The general assumption is that $a, b, c > 0$; $a = 10$, and c is varied [26]. The system exhibits chaotic behavior for $b = 28$, but displays knotted periodic orbits for other values of b . A saddle-node bifurcation occurs at $c(b - 1) = 0$. When $a \neq 0$ and $c(b - 1) \geq 0$, the equations generate three critical points. The critical points at $(0,0,0)$ correspond to no convection, and the critical points at $(\pm[c(b - 1)]^{0.5}, \pm[c(b - 1)]^{0.5}, b - 1)$ correspond to steady convection. This pair is stable only if $b < a(a + c + 3)/(a - c - 1)$. When $a = 10$, $b = 28$, $c = 8/3$, the Lorenz system has chaotic solutions, but not all solutions are chaotic.

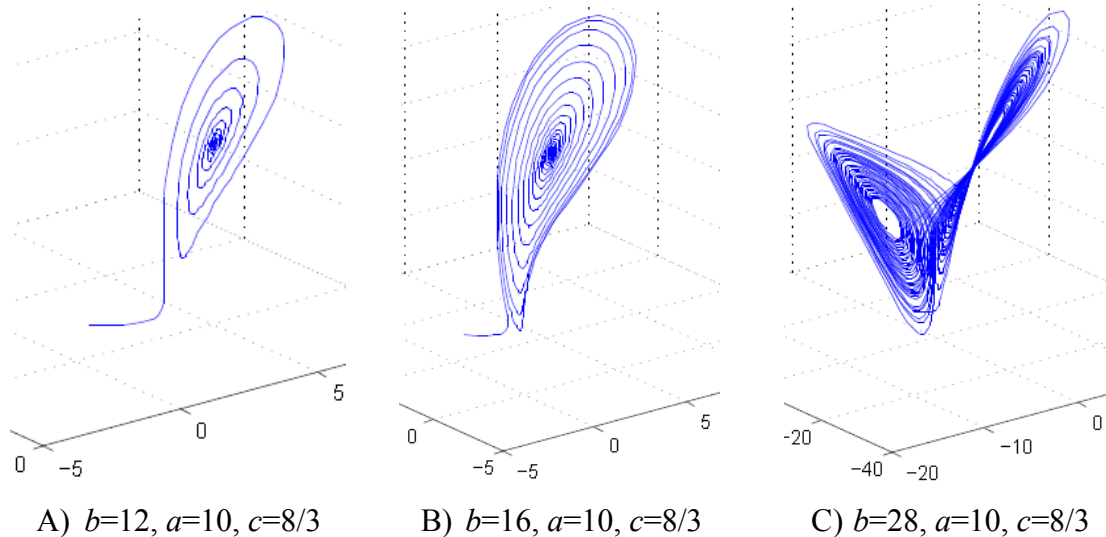


Figure 6. Solutions of the Lorenz system (Eqs. 20-22) for different values of b .

The Matlab calculations show the system evolution for different values of b (see Fig. 6). For small values of b , the system is stable and evolves to one of two fixed point attractors. When b is larger than 24.28, the fixed points become repulsors and the trajectory is repelled by them in a very complex way, evolving without ever crossing itself [26].

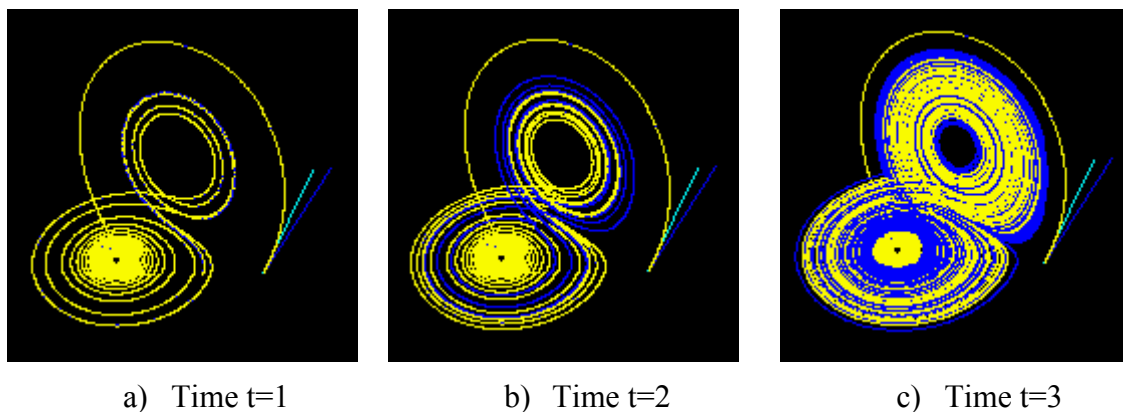


Figure 7. Sensitive dependence of the solution on initial condition at $a=10, b=28, c=8/3$.

Three time segments (received with the Java animation [27] and shown in Fig. 7 [26]) illustrate the 3-D evolution of two trajectories (one in blue and the other in yellow) in the

Lorenz attractor starting at two initial points that differ only by 10^{-5} in the x-coordinate. Initially, the two trajectories seem coincident (only the yellow one can be seen, as it is drawn over the blue one) but, after some time, the divergence is obvious [26].

6. Concluding Remarks on Students' Involvement

After in-class discussions of case studies, each student continued working on a selected case analyzing mathematical models, creating computer codes (in MATLAB, C/C++, Java, or FORTRAN), running them at various parameters, comparing computations with experimental data, and presenting the findings to classmates. In the course evaluations, students stated that they became deeply engaged in course activities through examining the challenging problems with the advanced math concepts and numerical algorithms.

References

- [1] Ascher, U.M., & Greif, C. *A First Course in Numerical Methods*. SIAM, 2011.
- [2] Riabov, V.V. *J. Comp. Sciences in Colleges*, 2012; 27(6): 58-60.
- [3] Dahlquist, G., & Björck, A. *Numerical Methods in Scientific Computing*. SIAM, 2008.
- [4] Casarin, R. *Monte Carlo Methods using Matlab*. [Online],
<http://www.venus.unive.it/r.casarin/Summer2012/SlidesCasarinMC.pdf>
- [5] Marchuk, G.I. *Methods of Computational Mathematics*. Moscow: Nauka, 1977.
- [6] Lebed, I.V., & Riabov, V.V. *J. Appl. Mech. Techn. Phys.*, 1983; 24(4): 447-454.
- [7] Riabov, V.V. *J. Thermophys. Heat Transfer*, 2000; 14(3): 404-411.
- [8] Brau, C.A., & Jonkman, R.H. *J. Chem. Phys.*, 1970; 52(2): 474-484.
- [9] Lordi, J.A., & Mates, R.E. *Phys. Fluids*, 1970; 13(2): 291-308.
- [10] Riabov, V.V. *Exploring Singular Differential Equations with Exponential Box-Scheme*. [Online] <http://archives.math.utk.edu/ICTCM/VOL19/C032/paper.pdf>
- [11] Riabov, V.V., & Provotorov, V. *J. Thermophys. Heat Transfer*, 1996, 10(1): 126-130.
- [12] El-Mistikawy, T.M., & Werle, M.J. *AIAA Journal*, 1978; 16(7): 749-751.
- [13] Doolan, E.P., Miller, J.J.H., & Schilders, W.H. A. *Uniform Numerical Methods for the Problems with Initial and Boundary Layers*. Dublin: Boole Press, 1980.
- [14] Schlichting, H. *Boundary-Layer Theory*, 7th edition. New York: McGraw-Hill, 1979.
- [15] Liu, T.M. & Chiu, H.H. *AIAA Journal*, 1976; 14(1): 114-116.
- [16] Keller, H.B. *SIAM Journal of Numerical Analysis*, 1974; 11(2): 305-320.
- [17] Provotorov, V.P. *Trudy TsAGI*, 1990; 2436: 165-173 (in Russian).
- [18] Riabov, V.V., & Provotorov, V.P. *J. Thermophys. Heat Transf.* 1995; 9(2):363-365.
- [19] Provotorov, V.P., & Riabov, V.V. *J. Appl. Mech. Techn. Phys.* 1987; 28(5):721-727.
- [20] Provotorov, V.P., Riabov, V.V. *Trudy TsAGI*, 1981; 2111: 142-156 (in Russian).
- [21] Ermakov, V.V., & Kalitkin, N.I. *J. Comput. Math. Math. Phys.* 1981; 21(2):235-242.
- [22] Johannesen, N., Bird, G.A., & Zienkiewicz, H.K. *J. Fluid Mech.* 1967; 30(1):51-64.
- [23] Hanson, R., Presley, L., & Williams, E. NASA TN D-6585, 1972.
- [24] Lorenz, E. N. *The Essence of Chaos*. Boca Raton, FL: CRC Press, 1995.
- [25] Lorenz, E. N. *J. Atmos. Sci.* 1963; 20(2): 130-141.
- [26] The Lorenz System. [Online] http://en.wikipedia.org/wiki/Lorenz_system/
- [27] Lorenz Attractor. [Online] http://to-campos.planetaclix.pt/fractal/lorenz_eng.html